Supporting Information for

Ultrathin PdPtP Nanodendrites as High-activity Electrocatalysts toward Alcohol Oxidation

Yan Zhang, [a] *Qiaoqiao Hao,* [a] *Jinyu Zheng,* [a] *Ke Guo* *[b], *Dongdong Xu* *[a]

[a]Jiangsu Key Laboratory of New Power Batteries, Jiangsu Collaborative Innovation Center of Biomedical Functional Materials, School of Chemistry and Materials Science, Nanjing Normal University, Nanjing, Jiangsu 210023, China.

E-mails: ddxu@njnu.edu.cn

[b]State Key Laboratory of Organic Electronics and Information Displays & Institute of Advanced Materials (IAM) Nanjing University of Posts & Telecommunications, Nanjing, Jiangsu 210023, China

E-mail: iamkguo@njupt.edu.cn

Experimental

Chemicals

Palladium chloride (PdCl$_2$, 99.9 wt%), Chloroplatinic acid hexahydrate (H$_2$PtCl$_6$·6H$_2$O, 99.9wt%), Sodium hypophosphate monohydrate (NaH$_2$PO$_2$•H$_2$O), ethanol, Potassium hydroxide (KOH, 95%), L-ascorbic acid (AA) were obtained from Sinopharm Chemical Reagent. Cetylpyridine chloride (C$_{16}$-py (Br$^-$)) and docosyl pyridine chloride (C$_{22}$-Py (Br$^-$)), N-(carboxymethyl)-N, N-dimethyldocosane-1-aminium bromide (C$_{22}$N-COOH (Br$^-$)), N-(carboxymethyl)-N, N-dimethyldocosane-1-aminium chloride (C$_{22}$N-COOH (Cl$^-$) didodecylpyridine bromide (C$_{22}$-Py (Br$^-$)), N-(carboxymethyl)-N, and N-1-dodecyl chloride (C$_{22}$N (Cl$^-$)) were synthesized according to our previously reported methods. H$_2$PdCl$_4$ (10 mM) solution was prepared by dissolving 0.355 g PdCl$_2$ in 20 mL HCl (0.2 M) solution and further diluting to 200 mL. All the above reagents were of analytical reagent grade and used without further purification.

Synthesis of PdPtP NDs and other nanodendrites

A mixed solution of H$_2$PdCl$_4$ (10 mM, 1.5 mL) and H$_2$PtCl$_6$ (10 mM, 500 μL) was added to a clear solution of surfactant (0.02 g C$_{22}$N-Py (Cl$^-$) dissolved in 5 mL of deionized water, after which 1 mL of freshly prepared AA (0.57 mM) was added and shaken homogeneously. The reaction solution was placed in an oven at 50°C, during which the solution changed from pink to blue-black. After 3 h, 500 μL NaH$_2$PO$_2$•H$_2$O (25 mM) was added to the above solution and the reaction was continued for 1.5 h at 95 °C. Finally, the PdPtP NDs products were collected by centrifugation and washed several times with ethanol. The other three dendritic nanocrystals (PdPt NDs, PdP NDs, and Pd NDs) were synthesized in a similar way to the above synthesis, except for the type of metal precursor and the surfactant concentration.

Electrochemical ethanol oxidation reaction measurements

Electrocatalytic EOR tests were carried out on a CHI 660E electrochemical workstation at room temperature (25 °C). A three-electrodes system was employed for all electrochemical tests, with a glassy carbon electrode (GCE) as the working electrode, a carbon rod as the counter electrode, and a saturated calomel electrode as the reference electrode. To prepare the ink of catalysts, 0.4 mg of catalyst and 1.6 mg of Vulcan XC-72 were mixed in 125 μL of ethanol and 75 μL of H$_2$O. After sonicating for 30 min, 10 μL of Nafion solution was added and further sonicated for another 30 min.

Then 1 μL of the ink solution (1 μg of the catalyst) was dropped on the GCE electrode and dried at 50 °C. The cyclic voltammogram (CV) curves were obtained in Ar-saturated 1.0 M KOH to evaluate the electrochemical active surface areas (ECSAs). The mass activity of catalysts was collected by scanning CV until a stable curve in Ar-saturated 1.0 M KOH and 1.0 M ethanol at a scan rate of 50 mV s^{-1}. To acquire the chronoamperometry curves, the catalysts electrode was tested in Ar-saturated 1.0 M KOH and 1.0 M ethanol mixture solution at the potential of -0.2 V *vs*. SCE for 5000 s. For the CO stripping tests, the catalysts electrode was scanned in 1.0 M KOH solution and purged with CO at 0.15 V for 30 min to cover the surface with CO. Then the electrode was transferred to another CO-free 1.0 M KOH solution for CO-stripping measurements in the potential range between -0.9 and 0.2 V *vs*. SCE. In this work, the mass activity was normalized to the mass of the sample, and the specific activity was normalized to the electrode area (0.0706 cm^2)

Characterizations

Transmission electron microscopy (TEM) observations and scanning transmission electron microscopy (STEM) mappings were performed on JEOL JEM-2100 and JEM-F200 with an accelerating voltage of 200 kV. TEM and STEM samples were prepared by casting a sample suspension onto a carbon-coated nickel grid (300 mesh). Wide-angle X-ray diffraction (XRD) patterns were obtained by using D/max 2500 VL/PC diffractometer (Japan) equipped with graphite-monochromatized Cu Kα radiation. X-ray photoelectron spectroscopy (XPS) was collected on a scanning x-ray probe (thermal ESCALAB 250 Xi) with Al Kα radiation. Inductively coupled plasma mass spectrometry (ICP-MS) was conducted on a NexION 350D.

Computational methods

Computational methods

The density functional theory calculations were performed by the Vienna ab initio simulation package Where the ion-electron interactions were modelled via the projector-augmented wave method. The exchange-correlation function was presented by the revised Perdew-Burke-Ernzerhof function. The plane wave cutoff energy was fixed at 400 eV in all calculations. The energy convergence threshold is 5×10^{-5} eV and all systems were relaxed until the force is less than 0.05 eV/Å. The k-space samplings of 3×3×1 was employed for geometry optimizations. Finally, a vacuum layer was set to be 15 Å to eliminate the interactions.
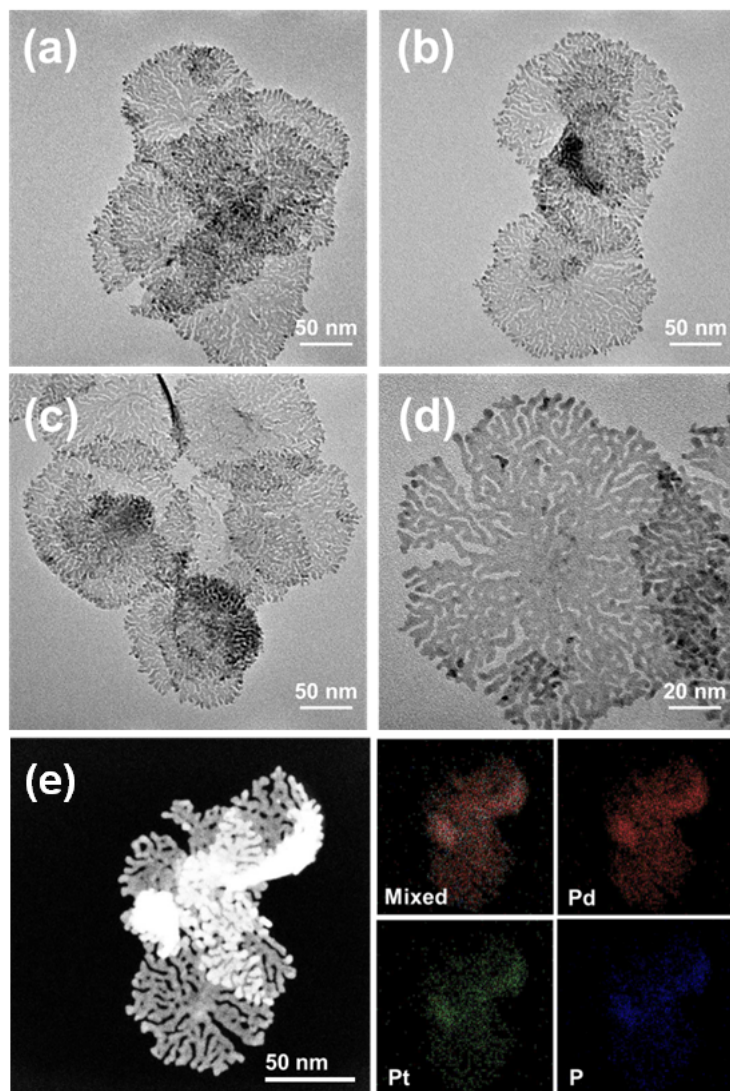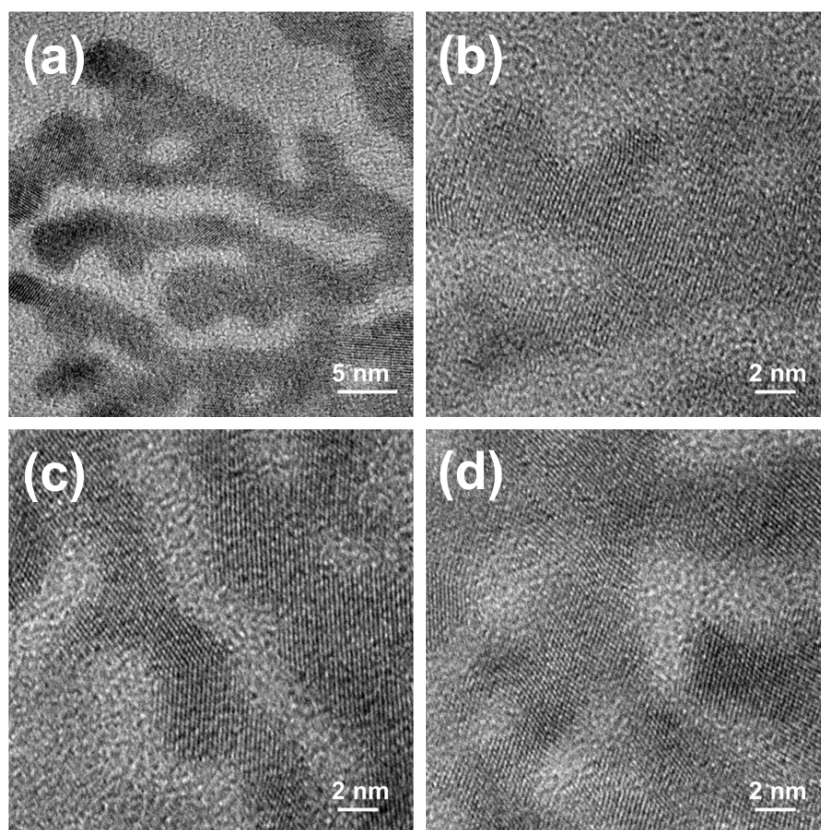
Figure S1. Additional TEM (a-d) and HAADF-STEM and elemental mapping (e) images of PdPtP NDs.
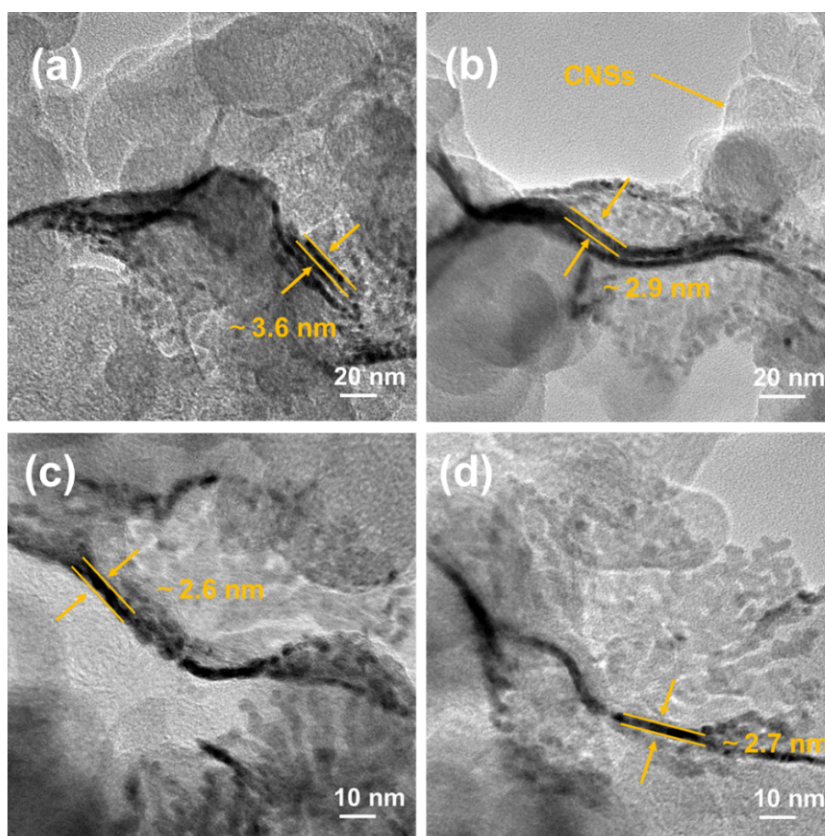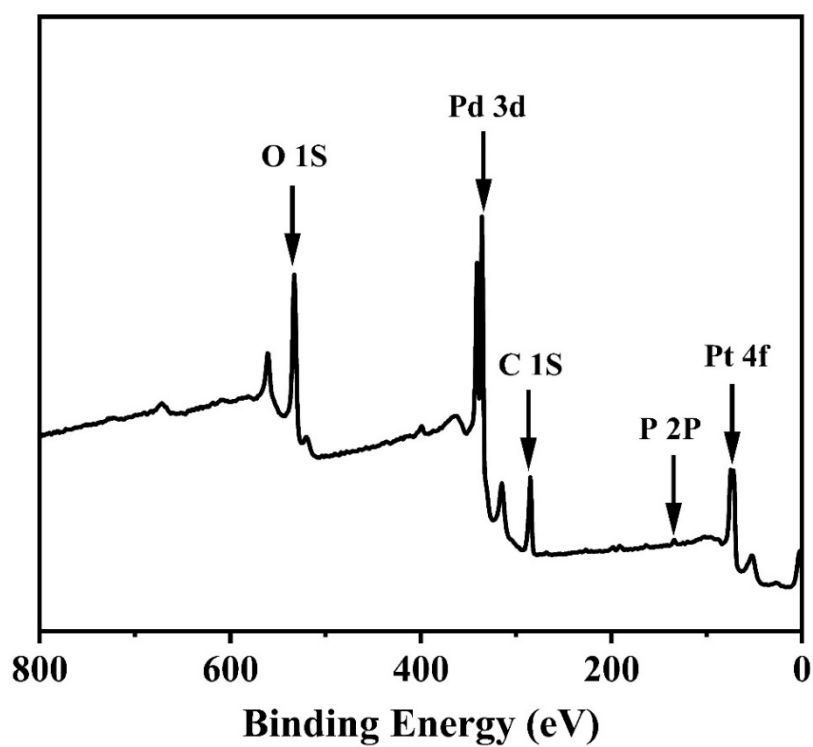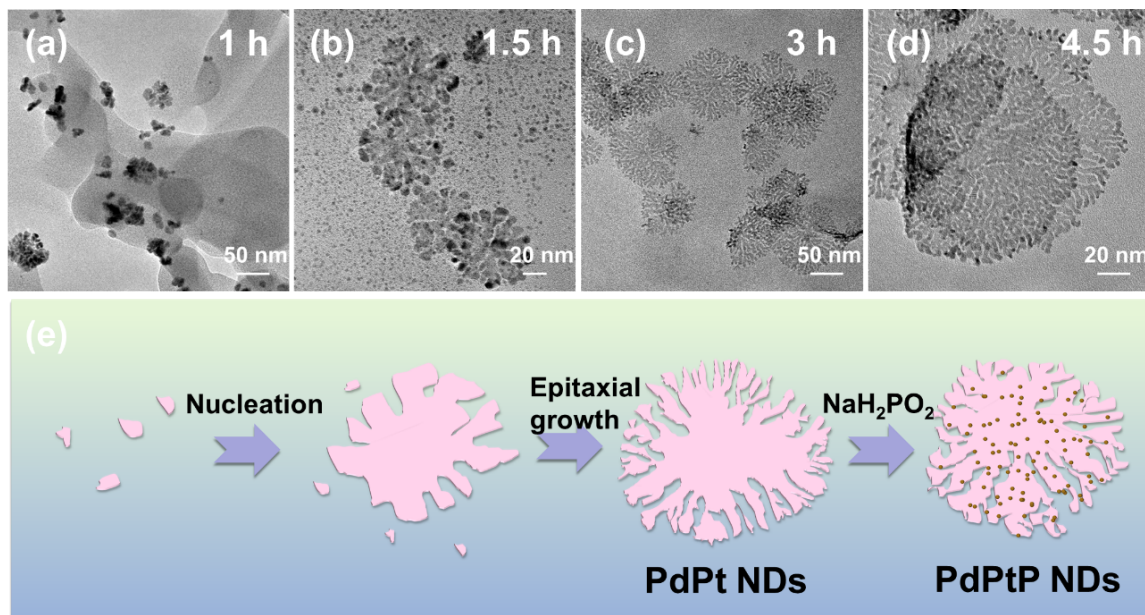
Figure S2. TEM images for the thickness of PdPtP NDs.

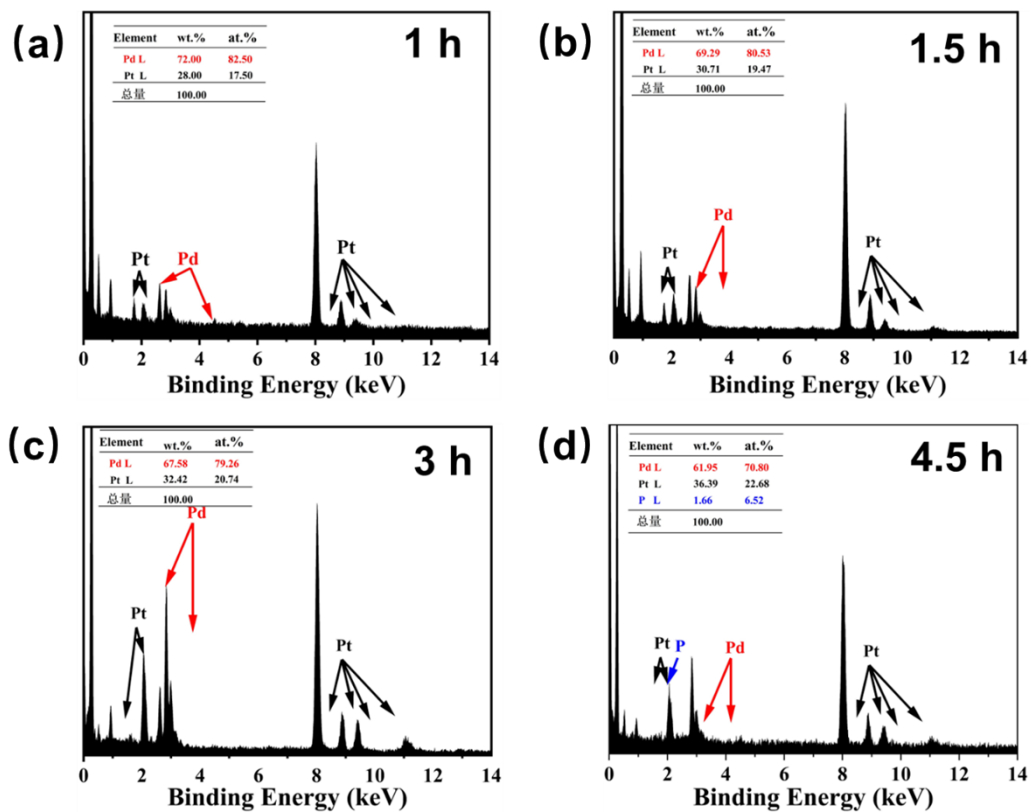**Figure S3.** Additional HRTEM images of PdPtP NDs.
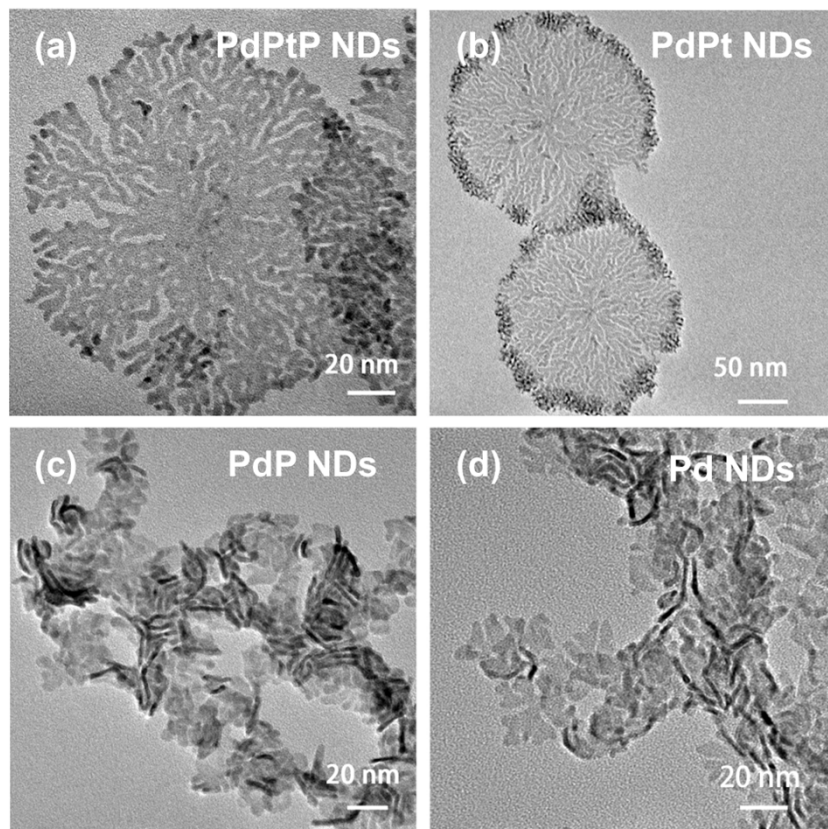
Figure S4. XPS survey of PdPtP NDs.

Figure S5. (a-d) Low-magnification TEM images and (e) schematic illustration of the formation of PdPtP NDs in different times.
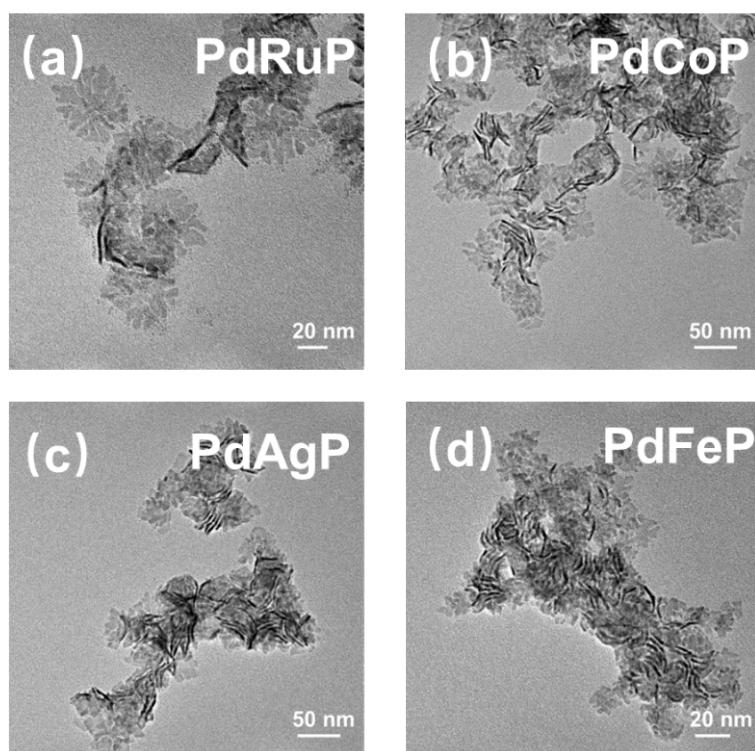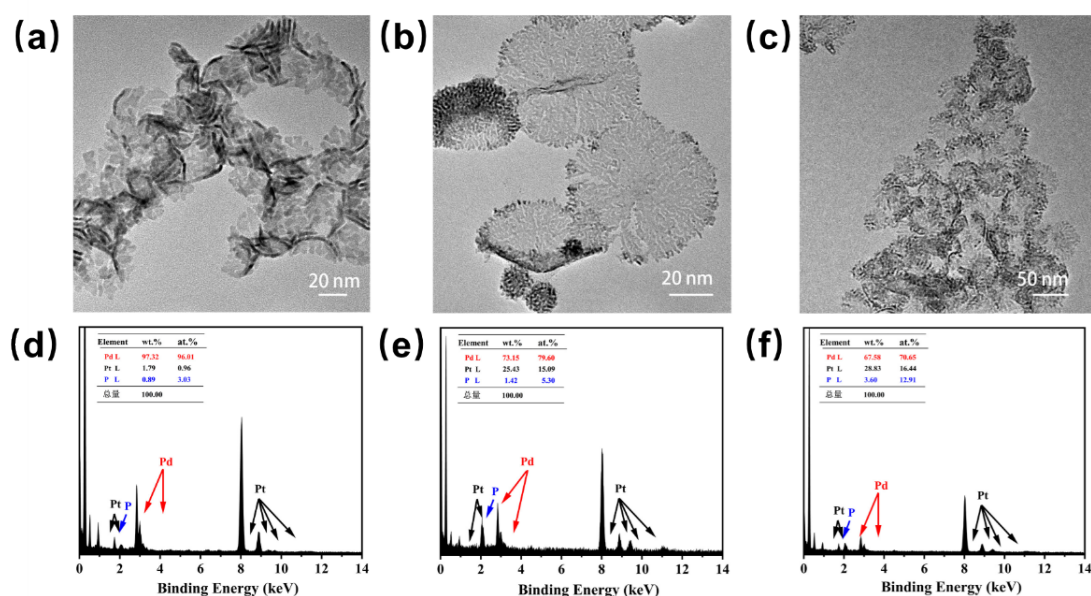
Figure S6. Low-magnification EDS of PdPtP NDs at different times.

Figure S7. The TEM of (a) PdPtP NDs, (b) PdPt NDs, (c) PdP NDs, and (d) Pd NDs, respectively.
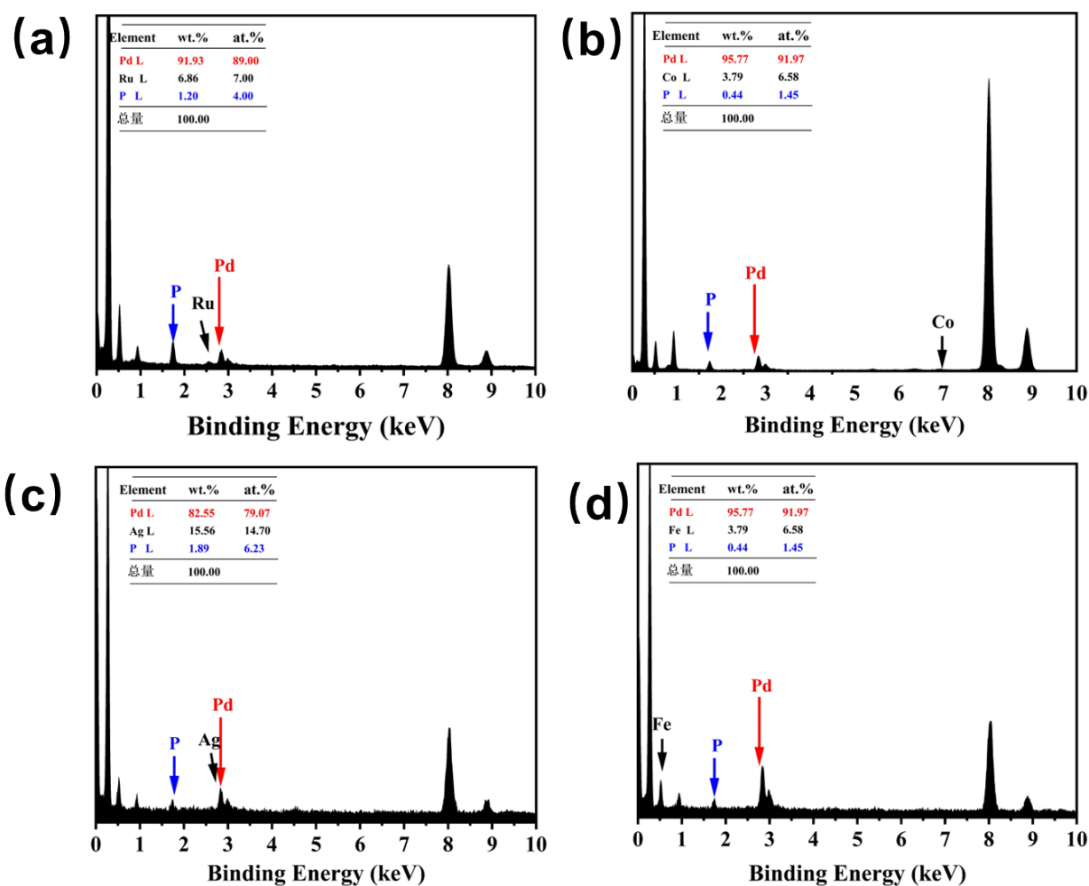
Figure S8. The TEM of (a) PdRuP, (b) PdCoP, (c) PdAgP, and (d) PdFeP, respectively.

Figure S9. TEM images and corresponding EDS analysis of $Pd_{96.01}Pt_{0.96}P_{3.03}$ NDs (a-d), $Pd_{79.6}Pt_{15.09}P_{5.30}$ NDs (b-e), and $Pd_{70.65}Pt_{16.44}P_{12.91}$ ND (e-f).

When we adjusted the content of Pt in the PdPtP NDs, as shown in **Fig. S9**, it was found that the degree of branching increased with the increase of Pt incorporation. Because of that, it can be proved that the doping of Pt has a crucial role in obtaining highly branched nanodendrites.

Figure S10. The EDS of (a) PdRuP, (b) PdCoP, (c) PdAgP, and (d) PdFeP, respectively.

Studying the growth of crystals at different time scales is an important step for probing the growth mechanism. In this work, we collected samples at 1 h, 1.5 h, 3 h, and 4.5 h (**Fig. S5**), and analyzed the structures and compositions of the samples at different reaction stages by TEM and EDS, respectively. The results show that with a reaction time of 1 h, PdPt nanoparticle aggregates with a size of about 10 nm were formed, and the reduction ratio of Pd to Pt atoms during the reaction was 82.5:17.5 (**Fig. S6**). With the reaction time at 1.5 h, the PdPt nanoparticles continue to grow and evolve into 100 nm nanodendrites, with a large number of nanoparticles around the nanodendrites, but the degree of branching at this point is relatively small. As the reaction proceeds, epitaxial growth continues around the already formed nanodendrites. The reaction initially ends when it reaches 3 h, forming PdPt NDs with uniform size, high dispersion, and high degree of branching. Next, a certain amount of $NaH_2PO_2 \cdot H_2O$ solution is added to the reaction solution, and the reaction is carried out at 95 °C for 1.5 h, which leads to the production of PdPtP NDs with the size of about 150 nm. From the EDS results, it can be analyzed that in the initial stage of the reaction, Pd is more easily reduced, so the degree of branching is lower at 1 h. And when the late stage of the reaction as the content of Pd
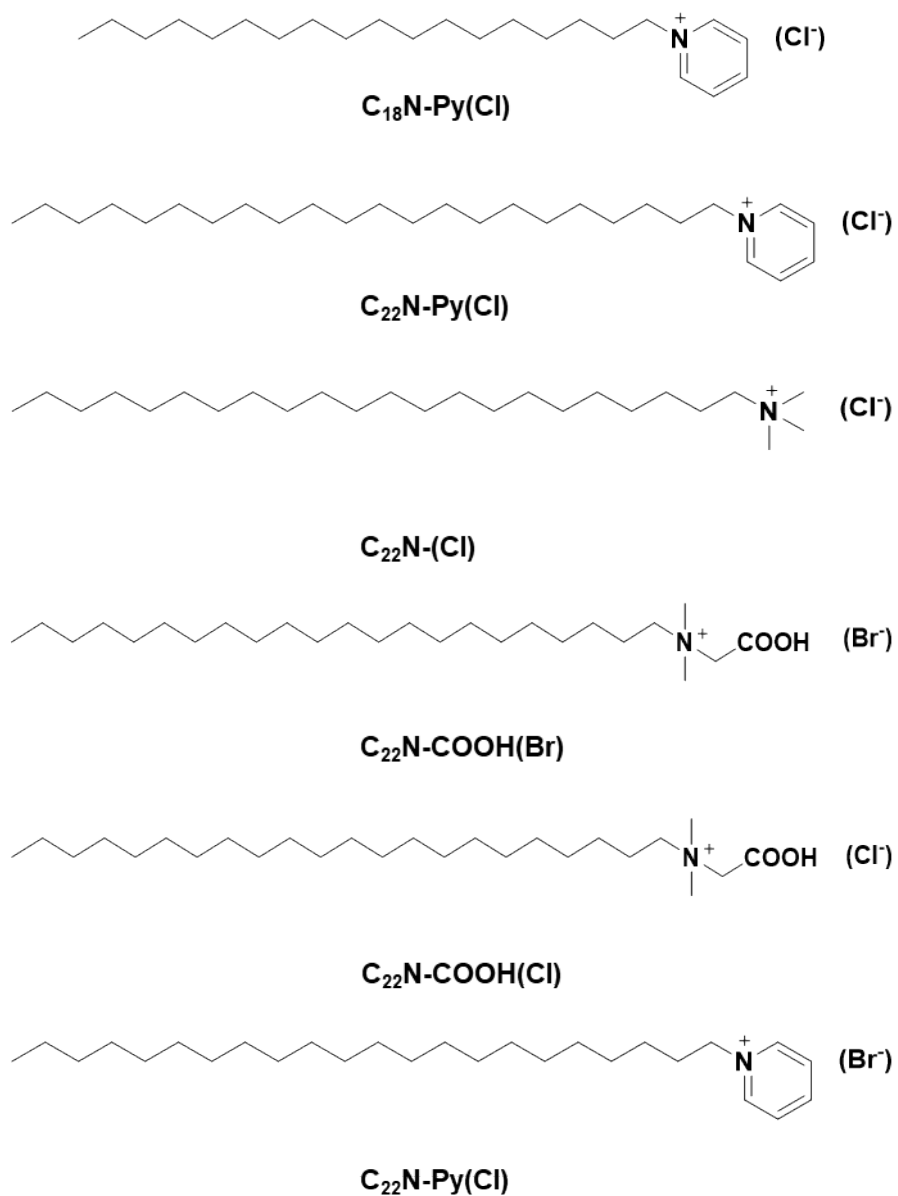
precursor decreases, more Pt precursors are reduced, which is shown as an increase in the degree of branching on the TEM image. Therefore, it is reasonable to speculate that the degree of branching is related to the reduction reaction of Pt. To test this conjecture, we performed a series of control experiments. First, we synthesized PdP NDs and Pd NDs without Pt, as shown in **Fig. S7**, and the resulting nanodendrites were low-branched 2D nanosheets. Whereas, replacing Pt with Ru, Co, Ag, and Fe, respectively (**Fig. S8 and S10**), similarly failed to obtain highly branched nanodendrites. When we adjusted the content of Pt in the PdPtP NDs, as shown in **Fig. S9**, it was found that the degree of branching increased with the increase of Pt incorporation. Because of that, it can be proved that the doping of Pt has a crucial role in obtaining highly branched nanodendrites.
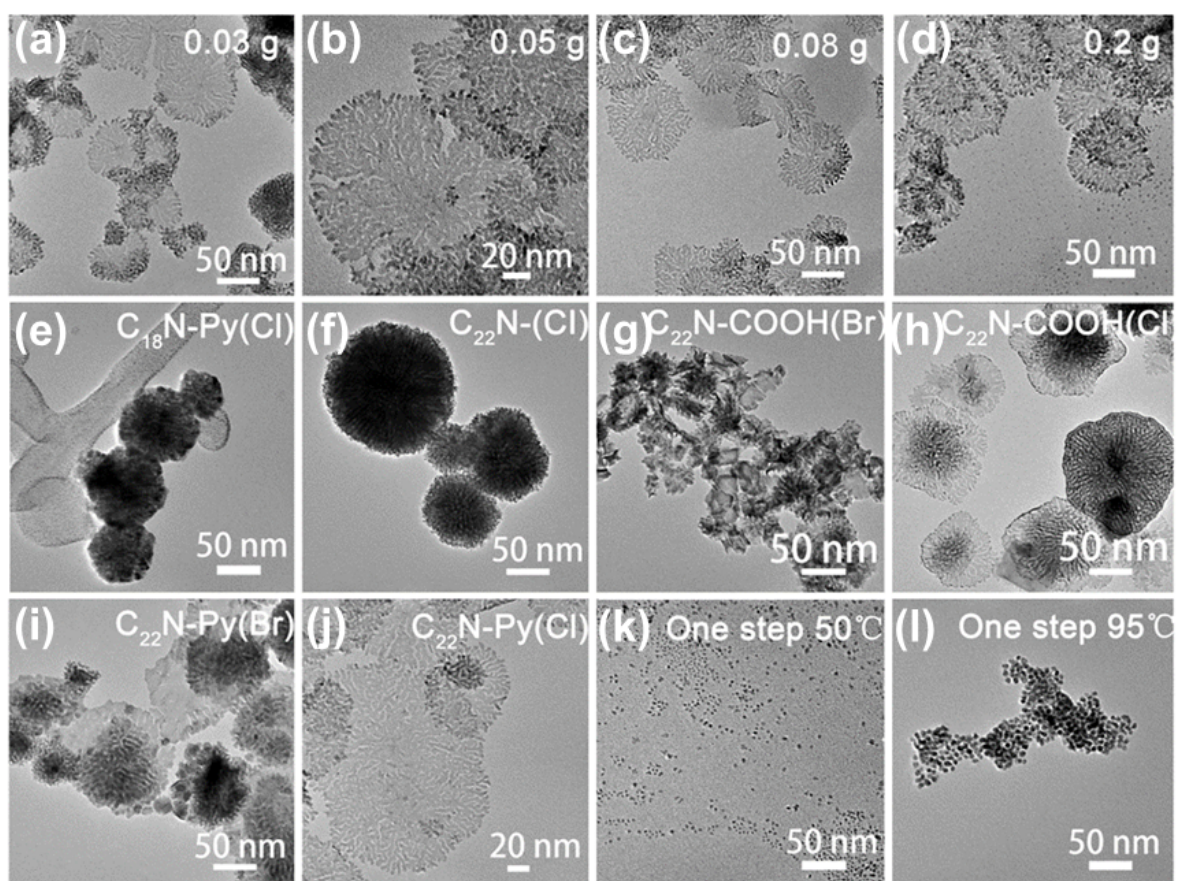
Figure S11. TEM images of PdPtP nanodendrites obtained under different synthesis conditions. (a-d) The different amounts of surfactants, (e-j) different types of surfactants, and (k-l) one-step phosphating at different temperatures.

In the synthesis system using soft template, the parameters of the surfactant have a great influence on the structure of the final product. The first one is the amount of surfactant as it is linked to the

micelle structure. As shown in **Fig. S11**, when the amount of surfactant added is in the range of 0.05 ~ 0.08 g, more uniform nanodendrites can be formed. When the addition amount is lower than 0.05 g, some three-dimensional nanodendrites are formed, which is due to the fact that the surfactant fails to fully assemble into stable lamellar micelles at this dose. And when the addition amount is 0.2 g, a large number of nanoparticles are formed around the nanodendrites due to the high concentration of organic substances, which hinders the oriented attachment between the particles. Subsequently, we adjusted the type of surfactant (see molecular configuration **Fig. S12**). As shown in **Fig. S11 (e-h)**, shorter alkyl chains, non-functional head groups, and carboxyl-type head groups are not favorable for the generation of two-dimensional structures, proving the importance of pyridyl functional head groups in this work. Besides, we also explored the effect of halogen ions. When $C_{22}N-Py$ (Br^-) was used, it was not favorable for the growth of 2D nanodendrites due to the rapid exchange of Br^- with $PdCl_4^{2-}$ in the reaction solution to form $PdBr_4^{2-}$, which has a relatively low reduction potential. As shown in **Fig. S11 (k-l)**, after a one-step phosphatization treatment at 50 °C and 95 °C, the product showed a nanoparticle structure, and no nanodendrites were formed (TEM images are shown in **Fig. S13-14**).

$C_{18}N\text{-Py(Cl)}$

$C_{22}N\text{-Py(Cl)}$

$C_{22}N\text{-(Cl)}$

$C_{22}N\text{-COOH(Br)}$

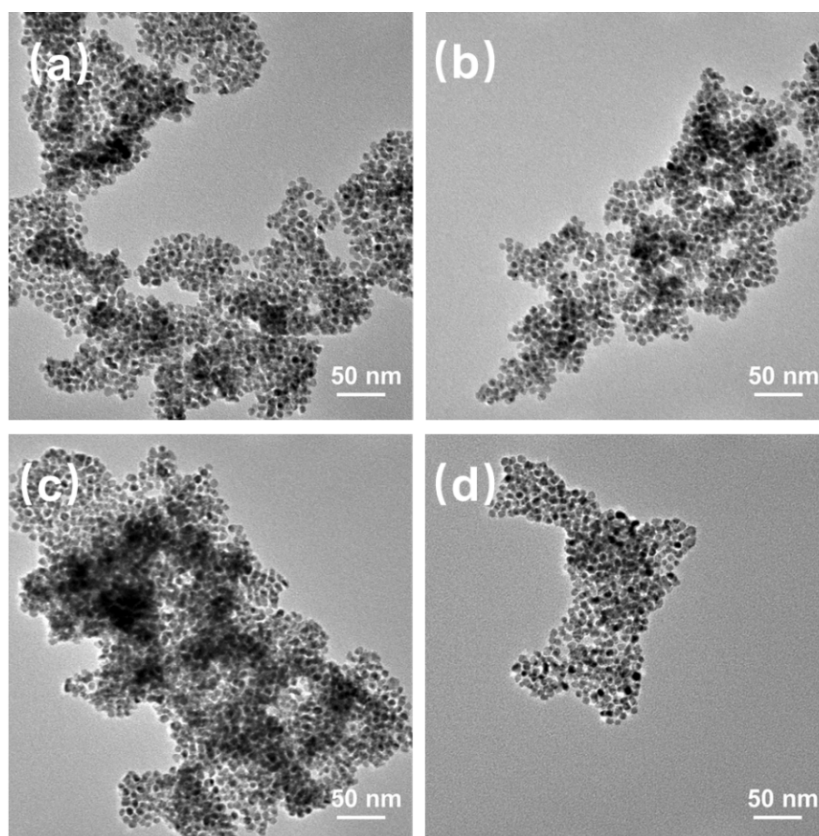$C_{22}N\text{-COOH(Cl)}$

$C_{22}N\text{-Py(Cl)}$

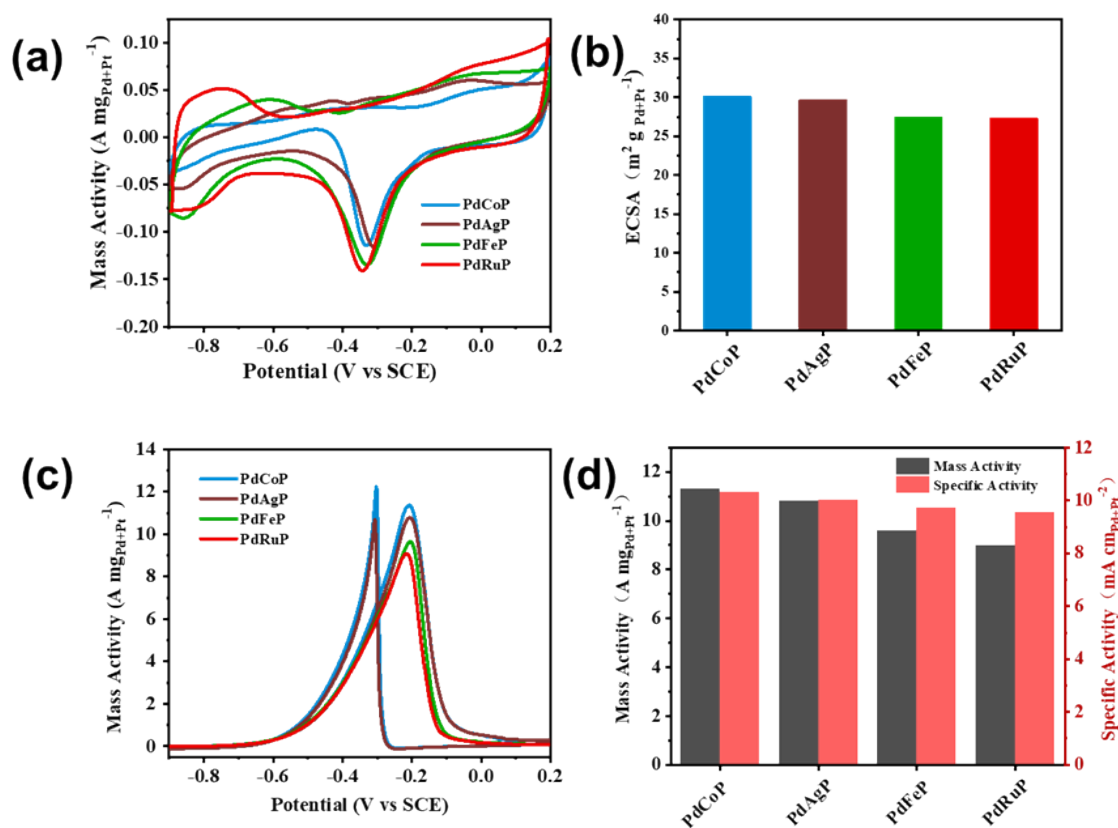**Figure S12.** Molecular structures of surfactants used in the synthesis.
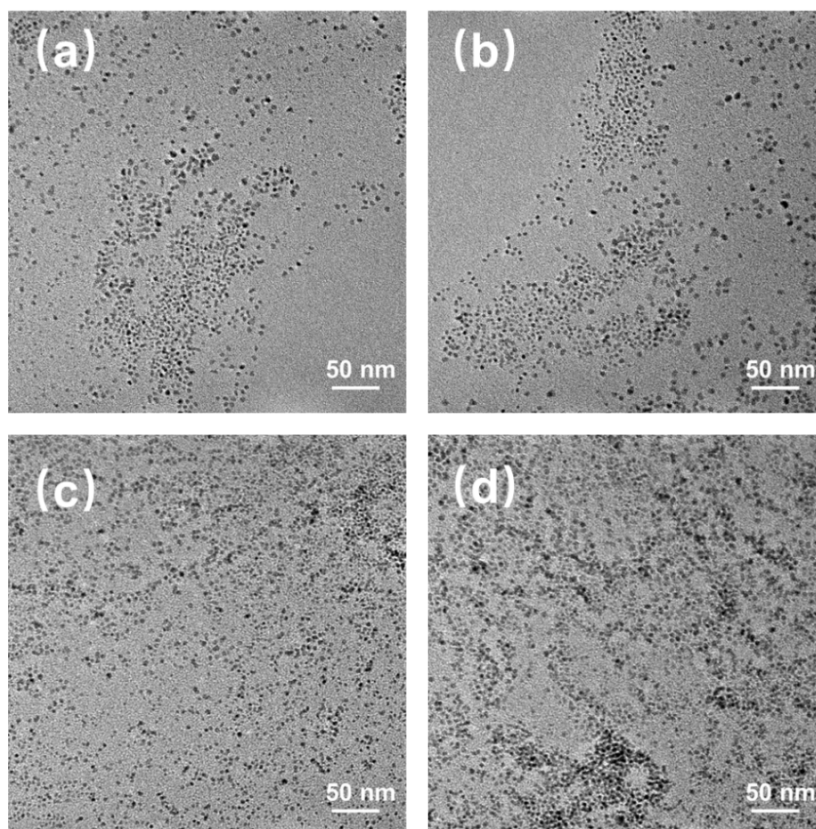
Figure S13. TEM images of PdPtP crystals obtained by one-step phosphatization at 50 °C.


Figure S14. TEM images of PdPtP crystals obtained by one-step phosphatization at 95 °C.

Figure S15 (a) CV curves and (b) the corresponding ECSAs of PdCoP, PdAgP, PdFeP, PdRuP NDs collected in 1.0 M KOH. (c) CV curves and (d) summarized mass/specific activities of PdCoP, PdAgP, PdFeP, PdRuP NDs collected in 1.0 M KOH and 1.0 M ethanol.

CV curves of PdRuP, PdCoP, PdAgP and PdFeP NDs were obtained in N_2 saturated 1.0 M KOH solution (Fig. S15). The results show that the four nanocatalysts have similar PdO peak areas in the range of -0.5V ~ -0.1V (relative to SCE). According to the integration of this region, the ECSAs of PdRuP, PdCoP, PdAgP and PdFeP are 27.04, 30.01, 29.61 and 27.42 $m^2g_{Pd+Pt}^{-1}$ (Fig. S15), all of which are lower than the ECSA of PdPtP NDs. The mass activity and specific activity of PdRuP, PdCoP, PdAgP, and PdFeP were determined in 1.0 M KOH and 1.0 M CH_3CH_2OH solutions at 25°C at potential -0.9 ~ 0.2 V (vs. SCE). The mass activity curves of several nanocatalysts showed that PdCoP NDs had the highest mass activity, and the mass activity of PdPtP NDs was 1.23, 1.32, 1.49 and 1.59 times that of PdRuP, PdCoP, PdAgP and PdFeP, respectively. The results show that doping of Pt not only enhances the branching degree of noble metal nanodendrites, but also enhances the ethanol oxidation performance of nanodendrites.
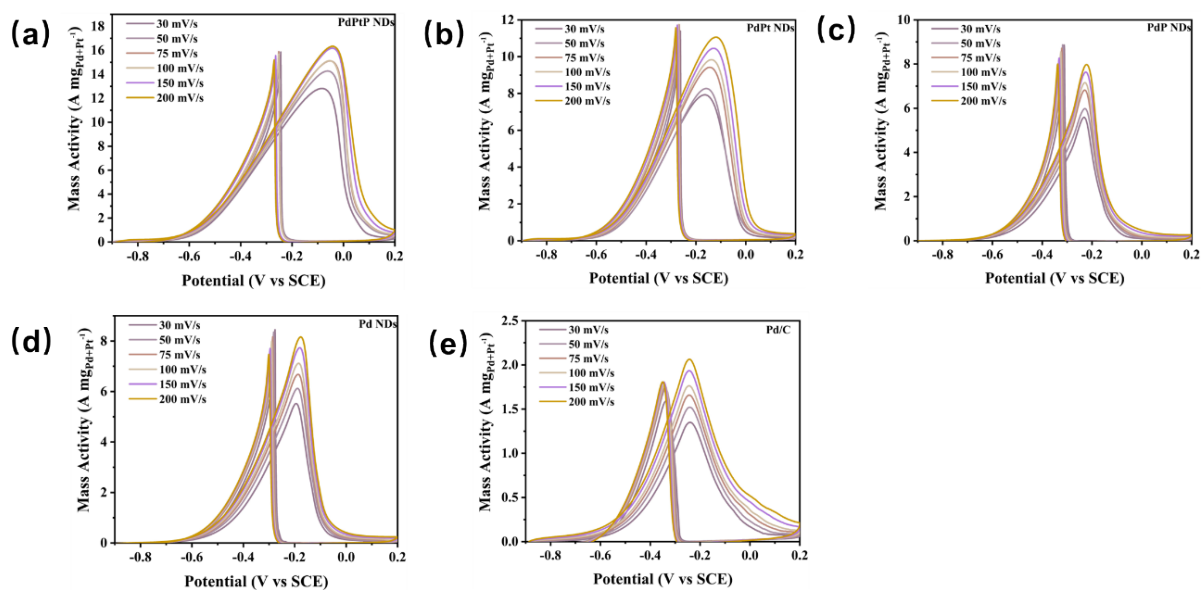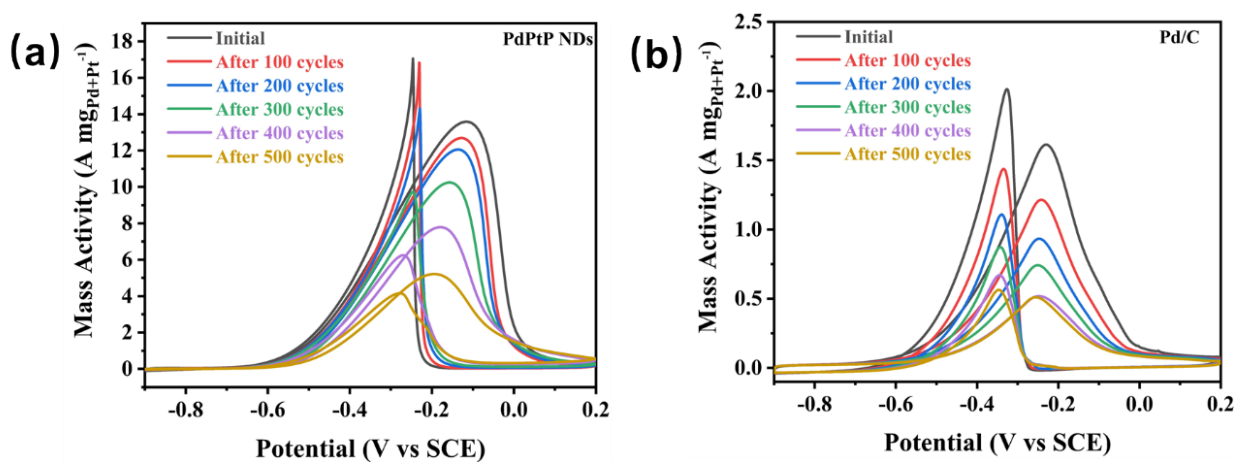
Figure S16. CV curves of PdPtP, PdPt, PdP, PdNDs, and commercial Pd/C collected in 1.0 M KOH and 1.0 M ethanol at different scanning rate.
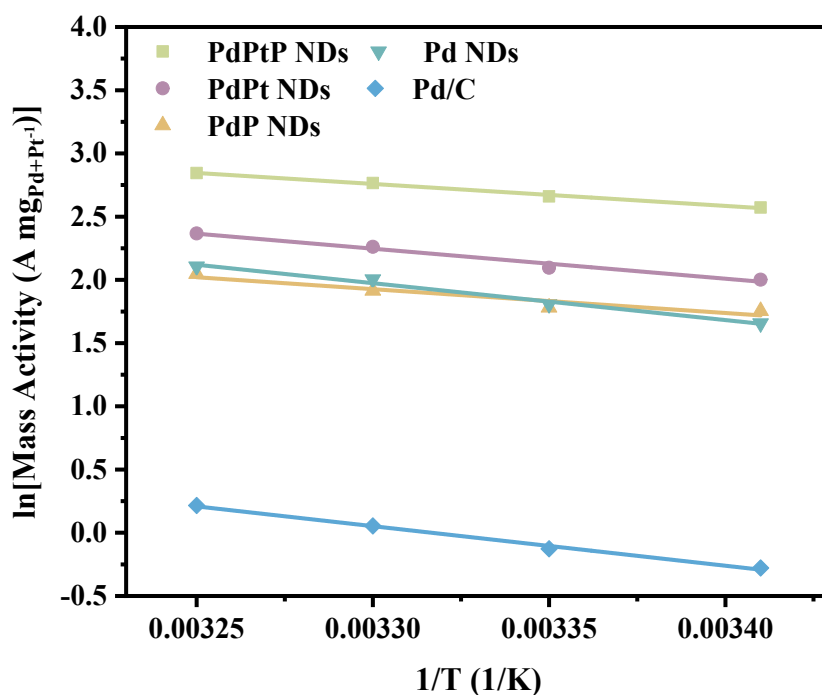
Figure S17. EOR kinetics based on mass activity and temperature of PdPtP, PdPt, PdP, Pd NDs, and commercial Pd/C.
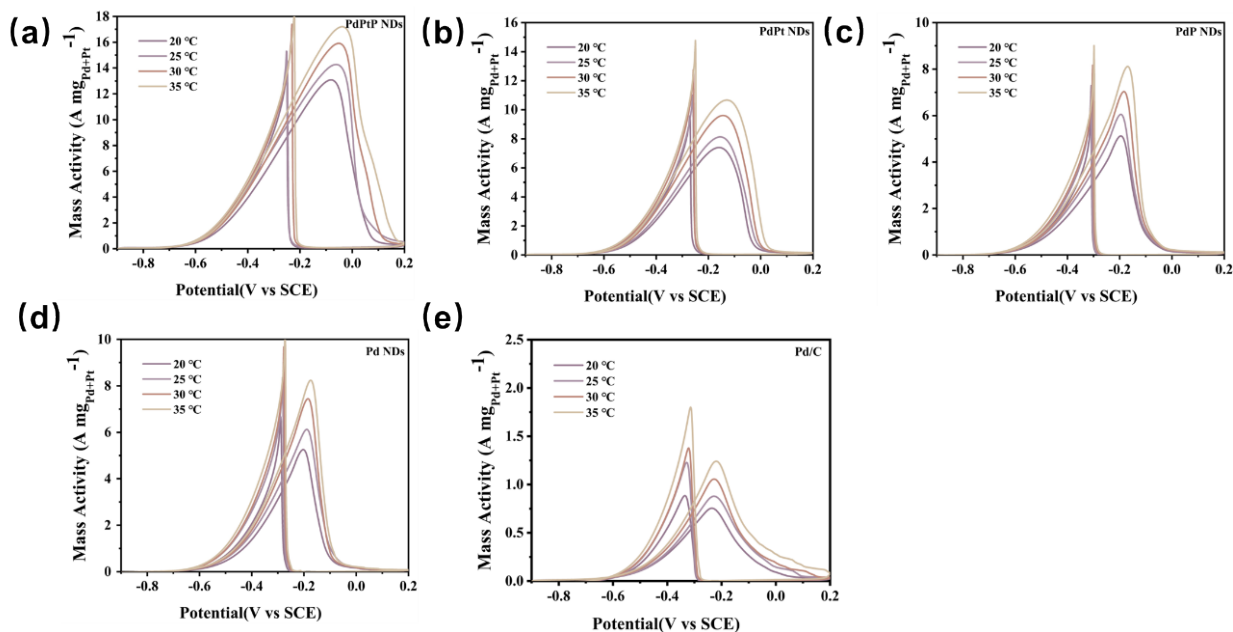
Figure S18. CV curves of PdPtP, PdPt, PdP, Pd NDs, and commercial Pd/C collected in 1.0 M KOH and 1.0 M ethanol at different temperature.

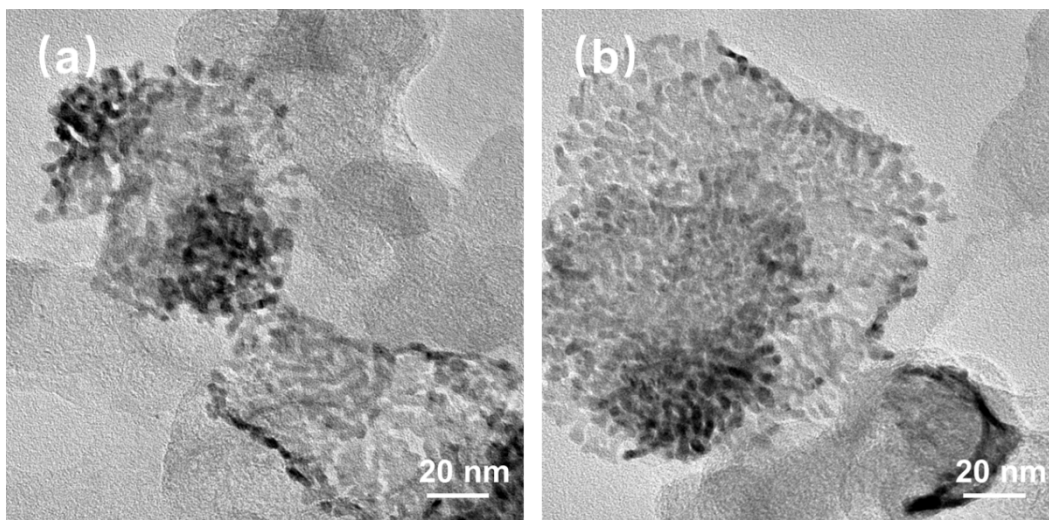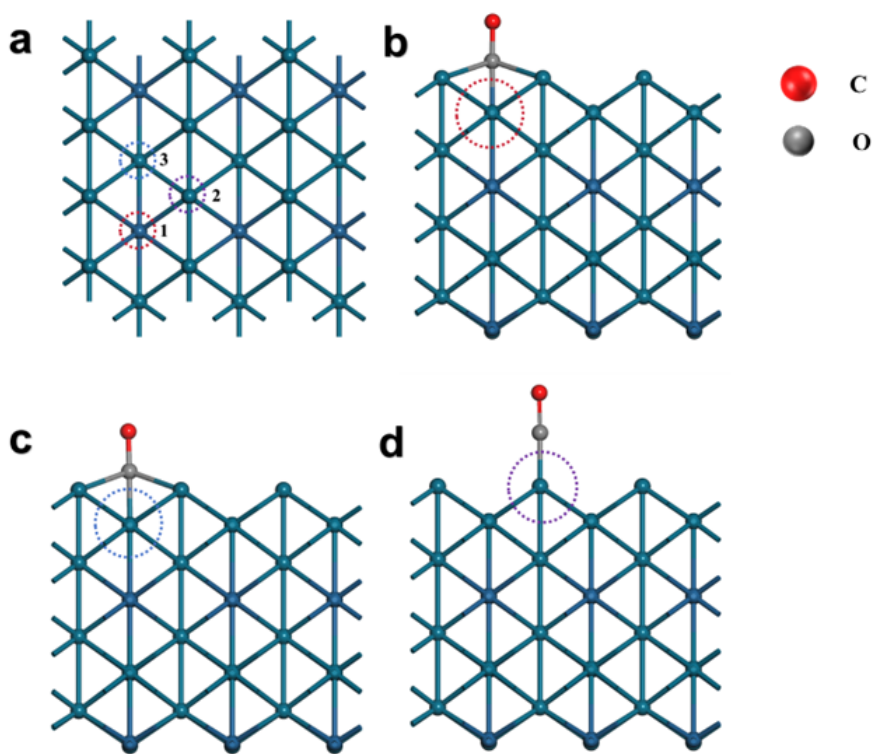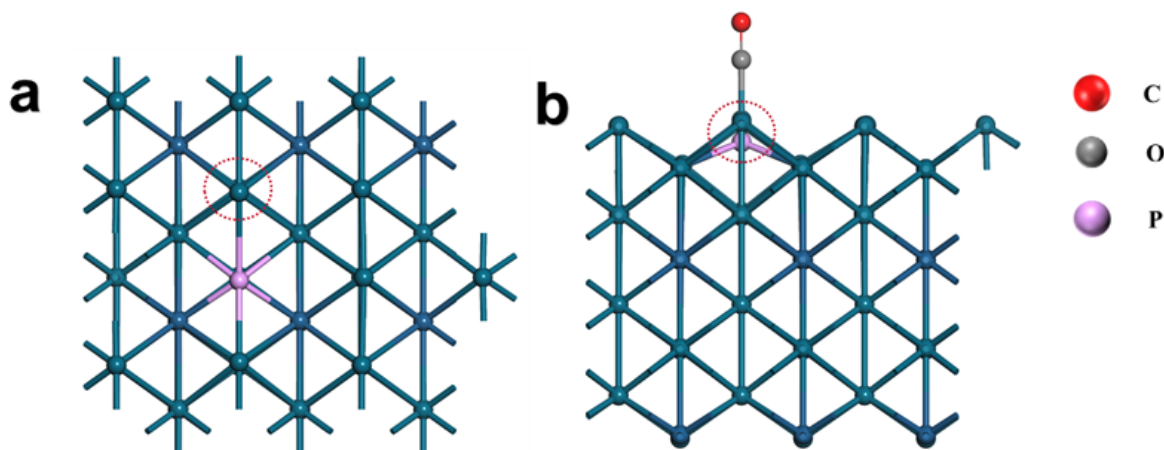**Figure S19.** CV curves of PdPtP NDs, and commercial Pd/C collected in 1.0 M KOH and 1.0 M ethanol after different cycles.

Figure S20. TEM images of PdPtP NDs after 5000 s chronoamperometric tests.

Figure S21. The configuration of PdPt NDs, (a)Top and (c-d) side view.

Figure S22. The configuration of PdPtP NDs (a)Top and (b) side view.

Here, we consider two models, one with undoped P atoms (Fig.S21) and one with doped P atoms (Fig.S22). Firstly, the adsorption energy of the catalyst without P for CO was investigated. The left side of Fig S21 is the top view, and the adsorption energy of Pt sites (Fig.S21 b-c) and Pd sites (Fig.S21 d) is calculated. The calculated results showed that the adsorption energy at the Pt site was low (-1.67 eV). Then, we compared the CO adsorption energy at the Pt site of the catalyst containing P (Fig. S22), and found that it was lower than the CO adsorption energy of the undoped P catalyst (-1.63eV), which proved that P doping reduced the CO adsorption energy on the surface of PtPdP NDs. This is consistent with the experimental results.
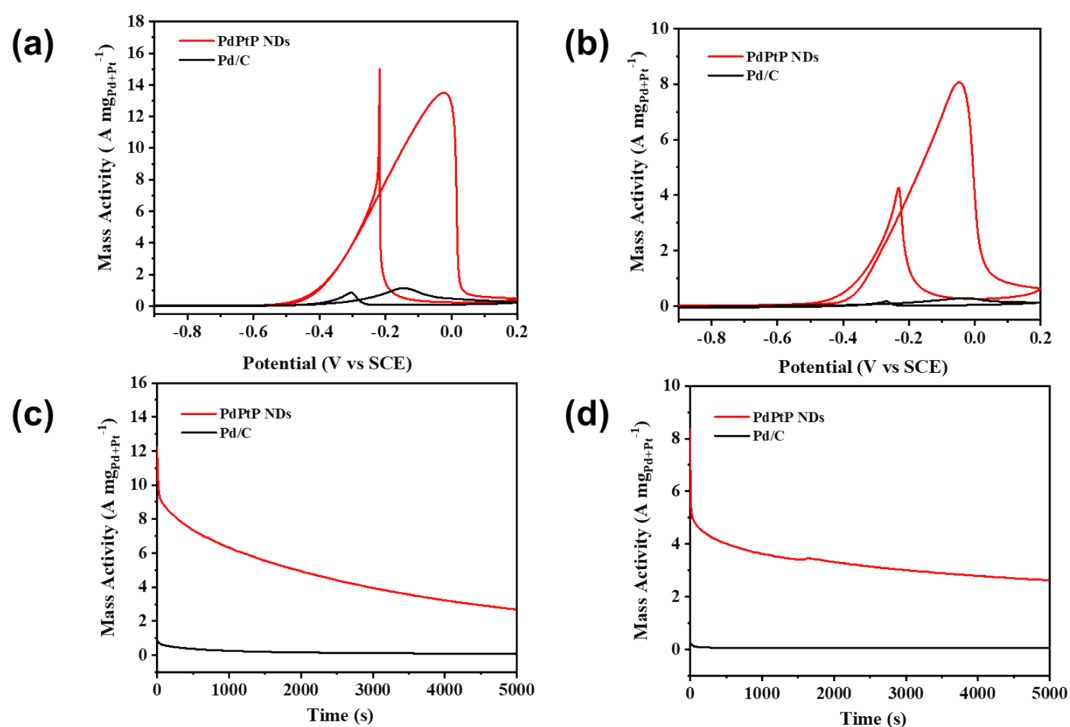
Figure S23. (a) CV curves and (c) i-t chronoamperometry curves of PdPtP NDs and Pd/C collected in 1.0 M KOH and 1.0 M ethylene glycol. (b) CV curves and (d) i-t chronoamperometry curves of PdPtP NDs and Pd/C collected in 1.0 M KOH and 1.0 M glycerol.
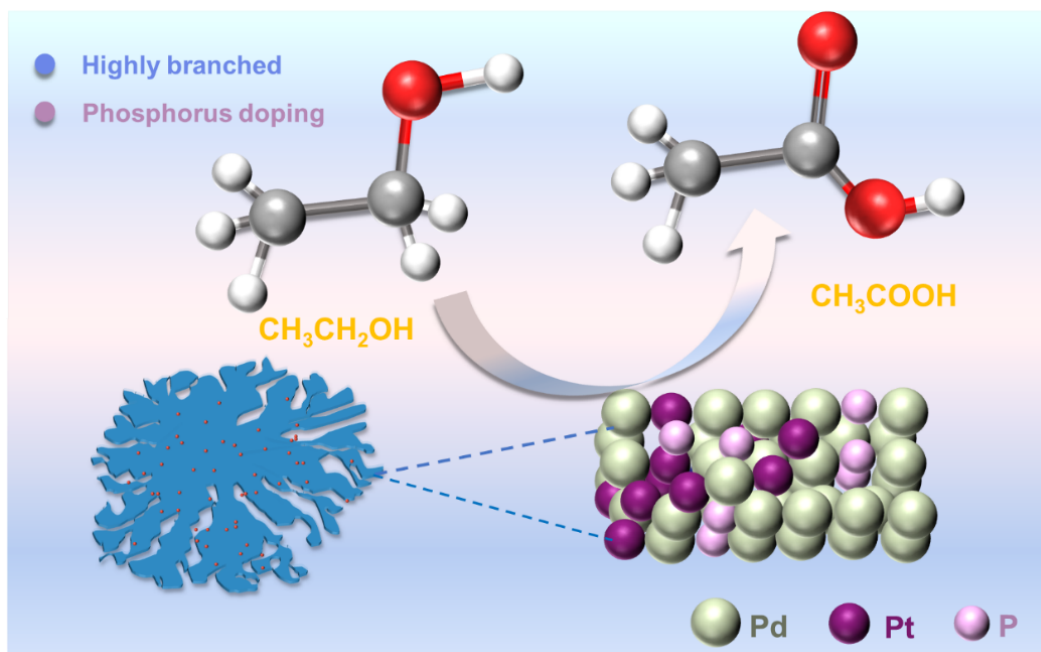
Figure S24. Schematic diagram of highly branched PdPtP nanodendrites improving electrocatalytic EOR performance

Based on the above electrochemical investigations, we propose possible mechanisms for PtPdP NDs for enhancing the catalytic performance of EOR (**Fig. S24**), including activity and stability. On the one hand, due to the introduction of Pt, the degree of branching of the nanodendrites becomes higher, which enhances the surface-to-volume ratio of the catalysts and facilitates the increase of the concentration of the active sites and thus the catalytic activity. On the other hand, the doping of P reduced the d-band center of the noble metal and enhanced the resistance to CO poisoning of the noble metal. At the same time, the P sites also facilitated the adsorption of OH_{ads} to optimize the further oxidation of CO_{ads} intermediates. Reducing the probability of the active site being poisoned definitely brings about the enhancement of stability. Thus, the highly branched geometrical features and the electronic structure properties of the ternary alloy synergistically and significantly enhance the EOR activity and stability of the PtPdP NDs.

Table S1. Summarization of EOR electrochemical performance of Pd-based and Pt-based nanocatalysts in alkaline solution.

Materials	Mass activity (A/mg)	ECSA (m^2/g)	Electrolyte	Scan rate (mV/s)	Reference
PdPtP NDs	14.3	32.4	1 M KOH +1.0 M ethanol	50	**This work**
PdP	4.06	55.9	1 M KOH +1.0 M ethanol	50	[1]
Pd NN	2.04	85.6	1 M KOH +1.0 M ethanol	50	[2]
Ag$_{49}$Pd$_{51}$ NPs	3.36	-	1 M KOH+ 1.0 M ethanol	50	[3]
Pd$_{50}$Ag$_{50}$	1.97	32.81	1 M KOH+ 1.0 M ethanol	50	[4]
CS$_{0.60}$Au@AgPd s-Ag$_{0.294}$Pd$_{0.706}$	1.16	77.5	0.3M KOH +0.5 M ethanol	-	[5]

Catalyst					
PdRuCu NAs	1.16	30.78	0.5M KOH+0.5 M ethanol	50	[6]
PtPd$_3$Ag$_5$/C-D	4.5	-	1 M KOH+ 1.0 M ethanol	50	[7]
Pd nanocages	3.765	91.3	1 M KOH+ 1.0 M ethanol	50	[8]
Pd$_{83}$Ni$_{17}$ HNS aerogel	3.630	55.5	1 M NaOH+ 1.0 M ethanol	50	[9]
IM-Pd$_3$Pb NNs	3.200	44.8	1 M KOH+ 1.0 M ethanol	50	[10]
Pd$_2$Ge Intermetallic Nanoparticles	-	14.1	1 M KOH+ 1.0 M ethanol	50	[11]
Pd nanoparticles supported on carbon nanotubes	2.939	89	1 M KOH+ 1.0 M ethanol	50	[12]
Pd$_1$Ni$_1$/C	2.37	67.3	1.0 M NaOH + 1.0 M ethanol	50	[13]
Pd$_{40}$Ni$_{43}$P$_{17}$	4.42	63.22	1.0 M NaOH + 1.0 M ethanol	100	[14]
FePd–Fe$_2$O$_3$/MWNTs	1.191	120.4	1.0 M NaOH + 1.0 M ethanol	50	[15]
Pd/TiO$_2$C	0.223	-	1.0 M KOH + 1.0 M ethanol	50	[16]

References

1. X. Yuan, B. Jiang, M. Cao, C. Zhang, X. Liu, Q. Zhang, F. Lyu, L. Gu and Q. Zhang, *Nano Res.*, 2020, **13**, 265-272.

2. H. Begum, M. S. Ahmed and S. Jeon, *ACS Appl. Mater.Interfaces*, 2017, **9**, 39303-39311.

3. X. Sun, Q. Qiang, Z. Yin, Z. Wang, Y. Ma and C. Zhao, *J Colloid Interf. Sci.*, 2019, **557**, 450-457.

4. S. Fu, C. Zhu, D. Du and Y. Lin, *ACS Appl. Mater.Interfaces*, 2015, **7**, 13842-13848.

5. T. Miao, Y. Song, C. Bi, H. Xia, D. Wang and X. Tao, *J.Phys.Chem.C*, 2015, **119**, 18434-18443.

6. R.-L. Zhang, J.-J. Duan, Z. Han, J.-J. Feng, H. Huang, Q.-L. Zhang and A.-J. Wang, *Appl. Surf. Sci.*, 2020, **506**, 144791.

7. Z. Yang, X. Wang, X. Kang, S. Zhang and Y. Guo, *Electrochim. Acta*, 2017, **236**, 72-81.

8. J. Sheng, J. Kang, Z. Hu, Y. Yu, X.-Z. Fu, R. Sun and C.-P. Wong, *J.Mater. Chem. A*, 2018, **6**, 15789-15796.

9. B. Cai, D. Wen, W. Liu, A.-K. Herrmann, A. Benad and A. *Angew. Chem. Int. Ed.*, 2015, **54**, 13101-13105.

10. Q. Shi, C. Zhu, C. Bi, H. Xia, M. H. Engelhard, D. Du and Y. Lin, *J. Mater. Chem. A*, 2017, **5**, 23952-23959.

11. S. Sarkar, R. Jana, Suchitra, U. V. Waghmare, B. Kuppan, S. Sampath and S. C. Peter, *Chem. Mater.*, 2015, **27**, 7459-7467.

12. M. S. Ahmed and S. Jeon, *J. Power Sources*, 2015, **282**, 479-488.

13. Z. Zhang, L. Xin, K. Sun and W. Li, *Int J Hydrogen Energ*, 2011, **36**, 12686-12697.

14. L. Chen, L. Lu, H. Zhu, Y. Chen, Y. Huang, Y. Li and L. Wang, *Nat. Commun.*, 2017, **8**, 14136.

15. Y. Wang, Q. He, J. Guo, J. Wang, Z. Luo, T. D. Shen, K. Ding, A. Khasanov, S. Wei and Z. Guo, *ACS Appl. Mater. Interfaces*, 2015, **7**, 23920-23931.

16. F. Hu, F. Ding, S. Song and P. K. Shen, *J Power Sources*, 2006, **163**, 415-419.